Soil-structure interaction in resonant railway bridges

A. Romero, M. Solís, J. Domínguez, P. Galvín

Escuela Técnica Superior de Ingeniería, Universidad de Sevilla, Camino de los Descubrimientos, 41092 Sevilla, Spain

Abstract

This paper explores dynamic soil-bridge interaction in high speed railway lines. The analysis was conducted using a general and fully three-dimensional multi-body finite element-boundary element model formulated in the time domain to predict vibrations caused by trains passing over the bridge. The vehicle was modelled as a multi-body system, the track and the bridge were modelled using finite elements and the soil was considered as a half-space by the boundary element method. The dynamic response of bridges to vehicle passage is usually studied using moving force and moving mass models. However, the multi-body system allows to consider the quasi-static and dynamic excitation mechanisms. Soil-structure interaction was taken into account by coupling finite elements and boundary elements. The paper presents the results obtained for a simply-supported short span bridge in a resonant regime under different soil stiffness conditions.

Key words: High speed train (HST), soil-structure interaction, railway bridge, resonant vibration

1. Introduction

In railway bridges, resonance occurs when the load frequency is equal to a multiple of the natural frequency of the structure. In short span bridges, the actual train operating speed can be close to resonance velocities. In that case, the high level vibrations reached in the resonance regime can lead to safety, passenger comfort and train stability problems. Therefore, the dynamic behaviour of railway bridges is an important design issue. The response of the structure is influenced by many factors such as soil properties, axle loads, geometry and mass characteristics of the train and track irregularities. These effects are evaluated by applying dynamic amplification factors to railway bridge standards, which represent the dynamic response amplification compared to the static response for a single moving load [1]. However, dynamic amplification factors do not account for resonance effects and their use is limited to train speeds below 220 km/h; in other cases, further analysis is needed.

References about the dynamic response of railway bridges are quite extensive. Frýba [2] developed a theoretical model of a bridge using the integral transformation method. This model provided an estimate

Email address: pedrogalvin@us.es (P. Galvín)

of the amplitude of free vibrations. Li and Su [3] studied the influence of vehicle-bridge interaction on resonant vibrations. They concluded that the maximum bridge response in the resonant regime is reached at the first resonance speed. Ju and Lin [4] proposed a three-dimensional finite element model to study resonance effects in multi-span bridges. They concluded that load frequencies and natural frequencies of bridges should be as different as possible to avoid resonance phenomena. Xia et al. [5] explored the resonance mechanisms and conditions of the train-bridge system, analysing the resonant regimes according to their excitation mechanisms.

Studying railway bridge vibrations requires an accurate model of the force induced by the train. Different vehicle models have been used: the moving load model, the moving mass model and moving oscillator models. The moving force model is the simplest vehicle model. It can be used if the train speed is low enough to neglect its inertia and has been widely employed by the engineering community [6, 7, 8, 9, 10]. The moving mass model is a more sophisticated model. It takes into account the mass of the vehicle but does not consider the effect of suspension. Finally, comprehensive moving oscillator models have been used by several authors [3, 4, 5, 11, 12]. Li and Su [3] established that the oscillator model leads to a lower response of the bridge than the moving force model due to the dynamic train-bridge interaction. Pesterev et al. [11] examined the asymptotic behaviour of the solution of the moving oscillator problem for large and small suspension stiffness values. A conclusion of that study was that the moving mass model is not equivalent to the moving oscillator model with infinite spring stiffness. Liu et al. [12] studied under which conditions the dynamic train-bridge interaction should be considered for the dynamic analysis of railway bridges. They concluded that the dynamic vehicle-bridge interaction is relevant for a large train-bridge mass ratio.

Little has been published about the influence of soil-structure interaction (SSI) on railway bridge response. Takemiya and Bian [13] and Takemiya [14] studied the soil-foundation-bridge interaction under moving loads using the substructure method in the frequency domain. They concluded that, in addition to train load profile, bridge geometry and soil properties, soil-structure interaction is crucial for determining the bridge and ground response. Recently, Ülker-Kaustell et al. [15] presented a qualitative analysis of the soil-structure dynamic interaction of a portal frame railway bridge. They concluded that the contribution of the soil-bridge interaction to the modal damping ratios is quite substantial in soft soils.

This paper presents the development of a three-dimensional numerical model to study the dynamic behaviour of a bridge accounting for soil-structure interaction (Fig. 1). The numerical model was based on a three-dimensional finite element and boundary element formulation in the time domain. The articulated train configuration was modelled as a multi-body system. The quasi-static and dynamic excitation mechanisms were considered. The outline of the paper is as follows: First, the numerical model is presented, including a brief summary of the finite element and the boundary element time domain formulations as well as the multi-body model used to represent the vehicle. Second, soil-structure interaction is analysed in a short span railway bridge. Changes in modal parameters are analysed considering the effect of the soil.

Next, induced vibrations are computed for several train speeds. Resonant and non-resonant regimes are studied. Finally, deck and support abutments are analysed for different soil types.

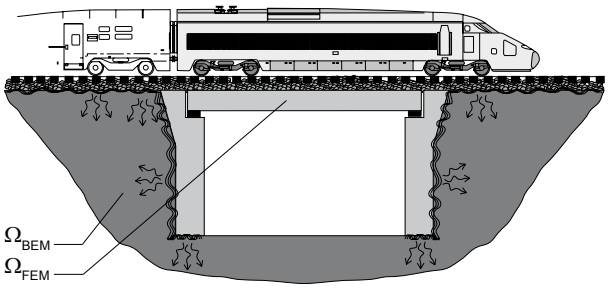

Figure 1: Vehicle-track-soil-structure interaction

2. Soil-structure interaction model

The dynamic response of a structure is considerably affected by the underlying soil. A homogeneous soil causes damping effects due to wave radiation to infinity [16]. The present study used three-dimensional finite element [17] and boundary element [18] time domain formulations to explore soil-structure behaviour.

The boundary element method system of equations can be solved step by step to obtain the time variation of the boundary unknowns (i.e., displacements and tractions). Piecewise constant time interpolation functions are used for tractions and piecewise linear functions are used for displacements. Nine-node rectangular quadratic elements are used for spatial discretization. Explicit expressions of the fundamental solution of displacements and tractions corresponding to an impulse point load in a three-dimensional elastic full-space can be seen in reference [19].

After performing the spatial and temporal discretization, the following equation is obtained for each time step:

$$\mathbf{H}^{nn}\mathbf{u}^{n} = \mathbf{G}^{nn}\mathbf{p}^{n} + \sum_{m=1}^{n-1}(\mathbf{G}^{nm}\mathbf{p}^{m} - \mathbf{H}^{nm}\mathbf{u}^{m})\exp\left[-2\pi\alpha(n-m)\Delta t\right] \tag{1}$$

where $\mathbf{u}^{n}$ is the displacement vector and $\mathbf{p}^{n}$ is the traction vector at the end of the time interval n, and $\mathbf{H}^{nn}$ and $\mathbf{G}^{nn}$ are the fully unsymmetrical boundary element system matrices in the time interval n, α is the soil attenuation coefficient and Δt is the time step [20].

The equation that results from the finite element method can be expressed symbolically as follows if the implicit Newmark time integration method is applied [21]:

$$\mathbf{D}^{nn}\mathbf{u}^{n} = \mathbf{f}^{n} + \mathbf{f}^{n-1} \tag{2}$$

where $\mathbf{D}^{nn}$ is the dynamic stiffness matrix, $\mathbf{u}^{n}$ is the displacement vector and $\mathbf{f}^{n}$ is the equivalent force vector at the end of the time interval n.

In this paper, the damping matrix $\mathbf{C}$ was considered proportional to the mass matrix $\mathbf{M}$ and the stiffness matrix $\mathbf{K}$:

$$\mathbf{C} = \alpha_0 \mathbf{M} + \alpha_1 \mathbf{K} \tag{3}$$

α_0 and α_1 are obtained from the i-th (ζ_i) and j-th (ζ_j) modal damping ratios. The n-th modal damping ratio is [22]:

$$\zeta_n = \frac{\alpha_0}{2\omega_n} + \frac{\alpha_1 \omega_n}{2} \tag{4}$$

The i-th and j-th modes should be chosen to obtain the damping ratios for all modes that contribute to the response. If both modes have the same damping ratio ζ, the result is:

$$\alpha_0 = \zeta \frac{2\omega_i \omega_j}{\omega_i + \omega_j} \quad \alpha_1 = \zeta \frac{2}{\omega_i + \omega_j} \tag{5}$$

Finally, coupling boundary element and finite element sub-regions provides satisfying equilibrium and compatibility conditions at the interface between both regions, as shown in reference [23].

3. Vehicle model

The train type considered in this paper consisted of one front traction car, eight passenger cars and one rear traction car. Passenger cars adjacent to traction cars shared one bogie with the neighbouring passenger car, while central passenger cars shared both bogies with the neighbouring cars. Bogie distances and axle distances of the articulated HST were $L_a = 3\,\mathrm{m}$ and $L_b = 18.7\,\mathrm{m}$, respectively. The mechanical properties of the HST are summarised in Table 1.

Description	Name	Unit	Traction cars	Passenger cars
Mass of car body	M_c	kg	55790	24000
Mass of bogie	M_b	kg	2380	3040
Mass of wheel axle	M_w	kg	2048	2003
Car body inertia moment	J_c	$kg\,m^2$	1.15×10^3	1.48×10^3
Bogie inertia moment	J_b	$kg\,m^2$	1.48×10^6	2.68×10^3
Primary suspension stiffness	k_1	N/m	2.45×10^6	1.4×10^6
Secondary suspension stiffness	k_2	N/m	2.45×10^6	0.82×10^6
Primary suspension damping	c_1	Ns/m	20×10^3	10×10^3
Secondary suspension damping	c_2	Ns/m	40×10^3	48×10^3

Table 1: Mechanical properties of HST

The multi-body model used to represent the vehicle is shown in Fig. 2.(a). Axles and car bodies were considered to be rigid parts. Primary and secondary suspensions are represented by spring and damper elements [24].

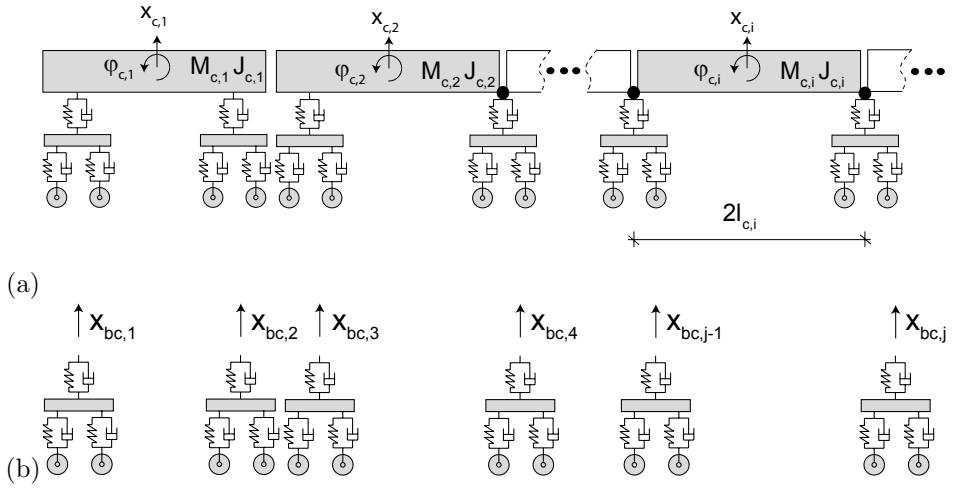

Figure 2: (a) Multi-body model of an articulated HST. (b) Uncoupled bogies.

The equations of motion for the uncoupled multi-body systems shown in Fig. 2.(b) can be written as follows:

$$\tilde{\mathbf{M}}\ddot{\mathbf{x}} + \tilde{\mathbf{C}}\dot{\mathbf{x}} + \tilde{\mathbf{K}}\mathbf{x} = \tilde{\mathbf{F}} \tag{6}$$

where $\tilde{\mathbf{M}}$, $\tilde{\mathbf{C}}$ and $\tilde{\mathbf{K}}$ are the mass, damping and stiffness matrices, respectively. Vehicle response is described by the displacement x_c and rotation φ_c of the body, the displacement x_b and rotation φ_b of the bogies and the displacement of the wheels x_{wr} and x_{wf} (Fig. 3).

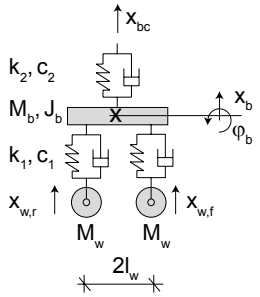

Figure 3: Multi-body model of a bogie

The mass matrix of each bogie (Eq. 7) is composed of the bogie mass M_b, the bogie inertia moment J_b and the wheel masses M_w:

$$\mathbf{M}_b = diag\,(0\ M_b\ J_b\ M_w\ M_w) \tag{7}$$

The stiffness and damping matrices of a bogie can be written as:

$$\mathbf{K}_b = \begin{pmatrix} k_2 & -k_2 & 0 & 0 & 0 \\ -k_2 & 2k_1+k_2 & 0 & -k_1 & -k_1 \\ 0 & 0 & 2k_1 l_w^2 & -k_1 l_w & k_1 l_w \\ 0 & -k_1 & -k_1 l_w & k_1 & 0 \\ 0 & -k_1 & k_1 l_w & 0 & k_1 \end{pmatrix} \quad \mathbf{C}_b = \begin{pmatrix} c_2 & -c_2 & 0 & 0 & 0 \\ -c_2 & 2c_1+c_2 & 0 & -c_1 & -c_1 \\ 0 & 0 & 2c_1 l_w^2 & -c_1 l_w & c_1 l_w \\ 0 & -c_1 & -c_1 l_w & c_1 & 0 \\ 0 & -c_1 & c_1 l_w & 0 & c_1 \end{pmatrix} \tag{8}$$

where k_1 and c_1 are the stiffness and damping of the primary suspension, k_2 and c_2 are the stiffness and damping of the secondary suspension, and $2l_w$ is the distance between the axles of a bogie.

The equation of motion of the whole train can be obtained from the displacement constraint equations between car bodies and bogies. The constraint equations used to obtain the equation of motion of the front traction car were [24]:

$$\begin{aligned} x_{bc,1} &= x_{c,1} - \varphi_{c,1} l_c \\ x_{bc,2} &= x_{c,1} + \varphi_{c,1} l_c \end{aligned} \tag{9}$$

where $x_{c,1}$ and $\varphi_{c,1}$ represent vertical displacement and rotation of the car body, respectively, and $2l_c$ represents the bogie distance in a vehicle. A similar expression can be drawn for the first passenger car (Fig. 2). The vertical displacement $x_{bc,n}$ of the m-th vehicle can be written as follows:

$$x_{bc,n} = 2\sum_{i=3}^{m} \left((-1)^{n+i} x_{c,i}\right) + (-1)^n \left(x_{c,2} + l_{c,2}\varphi_{c,2}\right) \tag{10}$$

The constraint equation for the whole train can be expressed as:

$$\mathbf{x}_{bc} = \mathbf{L}\mathbf{x}_c \tag{11}$$

Introducing Eq. (11) into Eq. (6) leads to the following equation:

$$\mathbf{M}\ddot{\mathbf{x}} + \mathbf{C}\dot{\mathbf{x}} + \mathbf{K}\mathbf{x} = \mathbf{F} \tag{12}$$

where $\mathbf{M}$, $\mathbf{C}$ and $\mathbf{K}$ are the mass, damping and stiffness matrices of the articulated HST (Fig. 2.(a)). The mass matrix is obtained by assembling the car body mass matrix:

$$\mathbf{M}_c = diag\left(M_c \; J_c\right) \tag{13}$$

where M_c is the mass of the car body and J_c is the inertia moment of the car body. The degree of freedom of rotation of the vehicle makes it possible to consider the pitch moment of inertia of the car directly.

Finally, the multi-body system was coupled with the soil-structure interaction model, imposing equilibrium and compatibility conditions at each wheel-rail contact point. A Hertzian contact spring was considered

between wheels and rails [24, 25]. As the vehicle moves along the track, contact points between wheels and rails change with time according to its speed. A moving node is created at each wheel-rail contact point in the rail to couple the vehicles and the track [23, 26]. Thus, the track mesh changes at each time step. Therefore, the mass, damping and stiffness matrices vary at each time step and the finite element system of equations obtained becomes non-linear. Nevertheless, the time domain formulation makes it possible to solve the non-linear system of equations [27].

Induced vibrations due to HST passage are generated by several excitation mechanisms: a quasi-static contribution, a parametric excitation due to the discrete support of the rails and a dynamic contribution. Usually, the quasi-static contribution is modelled as constant moving forces, neglecting the inertia effects of the vehicle. The multi-body system proposed in this paper allows considering the sprung and unsprung masses and the vehicle's suspension. The dynamic contribution accounts for track and wheel irregularities. Displacement u_c at the wheel-rail contact point is equal to the sum of rail displacement u_r due to the quasi-static contribution and the parametric excitation, and rail unevenness $u_{w/r}$ perceived by an axle [28, 29] in order to consider the unevenness:

$$u_c = u_r + u_{w/r} \tag{14}$$

Random track unevenness $u_{w/r}(y)$ was modelled as a stationary Gaussian random process characterized by its one-sided PSD function $\tilde{S}_{u_{w/r}}(k_y)$. The spectral representation theorem was used to generate samples of track unevenness $u_{w/r}(y)$ as a superposition of harmonic functions with random phase angles [28, 29]:

$$u_{w/r}(y) = \sum_{m=1}^{n} \sqrt{2\tilde{S}_{u_{w/r}}(k_{ym})\Delta k_y}\cos(k_{ym}y - \theta_m) \tag{15}$$

where $k_{ym} = m\Delta k_y$ is the wavenumber sampling used only to compute the artificial profile, Δk_y is the wavenumber step and θ_m are the independent random phase angles uniformly distributed in the interval $[0, 2\pi]$. The artificial track profile was generated from the PSD function following the ISO 8608 standard [30]:

$$\tilde{S}_{u_{w/r}}(k_y) = \tilde{S}_{u_{w/r}}(k_{y0})\left(\frac{k_y}{k_{y0}}\right)^{-w} \tag{16}$$

An artificial profile was obtained from the PSD function with $k_{y0} = 1\,\text{rad/m}$ and $\tilde{S}_{u_{w/r}}(k_{y0}) = 2\pi \times 10^{-8}\,m^3$. Wheel-rail unevenness in current high speed lines is commonly assumed to be $w = 3.5$.

4. High speed railway bridges

This section analyses the effect of soil-structure interaction on railway bridges. A simply supported 12 m long railway bridge was studied. The deck (Fig. 4.(a)) was composed of a 0.25 m thick concrete slab. The slab rested over five pre-stressed concrete beams with a 0.75×0.3 m rectangular cross-section. The distance between beams was 1.39 m. The concrete properties were the following: density $\rho = 2500\,\text{kg/m}^3$, Poisson's ratio $\nu = 0.2$ and Young's modulus $E = 31 \times 10^9\,\text{N/m}^2$.

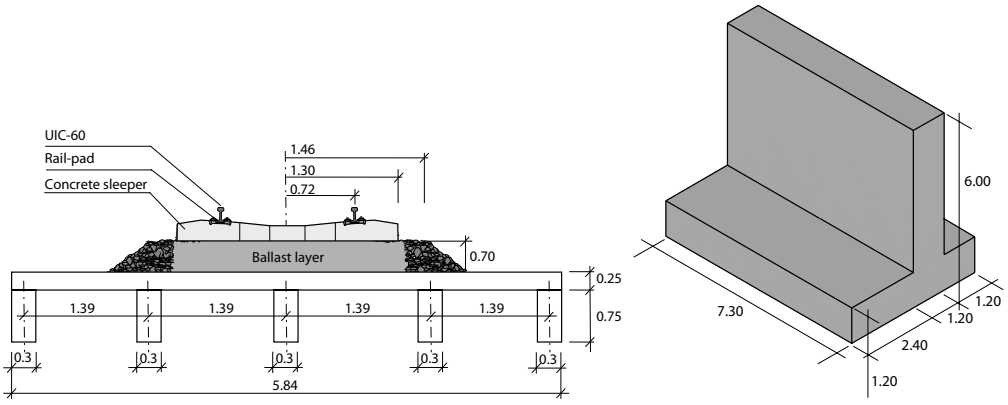

(a) (b)

Figure 4: (a) Deck cross-section. (b) Abutment geometry.

The deck leaned over two concrete abutments (Fig. 4.(b)) with the following properties: density $\rho = 2500\,\mathrm{kg/m^3}$, Poisson's ratio $\nu = 0.3$ and Young's modulus $E = 20 \times 10^9\,\mathrm{N/m^2}$. The beams rested on laminated rubber bearings. The thickness of the bearings was 20 mm and their stiffness and damping values were $k_b = 560 \times 10^6\,\mathrm{N/m}$ and $c_b = 50.4 \times 10^3\,\mathrm{Ns/m}$, respectively.

A single ballast track was located over the deck. The track was composed of two UIC60 rails with a bending stiffness $EI = 6.45 \times 10^6\,\mathrm{Nm^2}$ and a mass per unit length $m = 60.3\,\mathrm{kg/m}$ for each rail. The rail pads had a thickness of 10 mm and stiffness and damping values of $k_{rp} = 150 \times 10^6\,\mathrm{N/m}$ and $c_{rp} = 13.5 \times 10^3\,\mathrm{Ns/m}$, respectively. The pre-stressed concrete mono-block sleepers had the following characteristics: length $l = 2.50\,\mathrm{m}$, width $w = 0.235\,\mathrm{m}$, height $h = 0.205\,\mathrm{m}$ (under the rail) and mass $m = 300\,\mathrm{kg}$. A distance $d = 0.6\,\mathrm{m}$ between the sleepers was considered. The ballast had a density $\rho = 1800\,\mathrm{kg/m^3}$, Poisson's ratio $\nu = 0.2$, and Young's modulus $E = 209 \times 10^6\,\mathrm{N/m^2}$. The width of the ballast was 2.92 m and the height was $h = 0.7\,\mathrm{m}$.

The structure was assumed to be located on top of a half-space that represented the soil. The soil was a homogeneous viscoelastic soil with Poisson's ratio $\nu = 0.35$ and mass density $\rho = 1800\ \mathrm{kg/m^3}$. Four different S–wave velocities were analysed, corresponding to a soil with infinite stiffness ($C_s = \infty\,\mathrm{m/s}$), a stiff soil ($C_s = 400\,\mathrm{m/s}$), a medium soil ($C_s = 250\,\mathrm{m/s}$) and a soft soil ($C_s = 150\,\mathrm{m/s}$).

4.1. Soil-structure dynamic behaviour

Resonance in railway bridges occurs when the load frequency of the train becomes close to the natural frequency of the structure. For a resonant regime to begin, the structure also needs to be lightly damped.

Fig. 6 shows four natural frequencies and mode shapes of the structure: the first bending mode(symmetric), the first torsional mode, the first bending of cross-section mode (symmetric) and the first antisymmetric deck bending mode shape, respectively. At least, the contribution of the first symmetric and antisymmetric bending modes to the response of simply supported railway bridges should be considered [6]. Therefore,

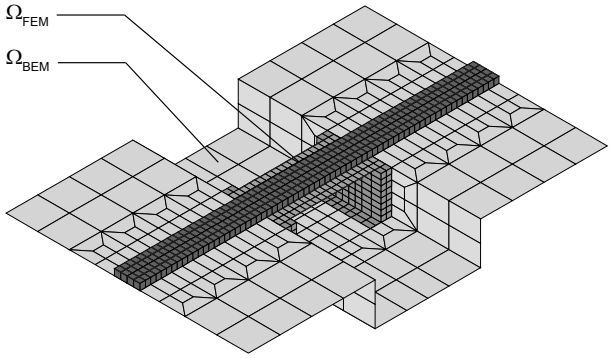

Figure 5: Soil-structure discretization

the finite element damping matrix (Eq. 2) is obtained by assigning the same damping ratio $\eta = 2\,\%$ to these modes considering $\omega_i = \omega_1$ and $\omega_j = \omega_4$. Rayleigh damping parameter values are $\alpha_0 = 2.3\,\mathrm{s}^{-1}$ and $\alpha_1 = 1.24 \times 10^{-4}\,\mathrm{s}$.

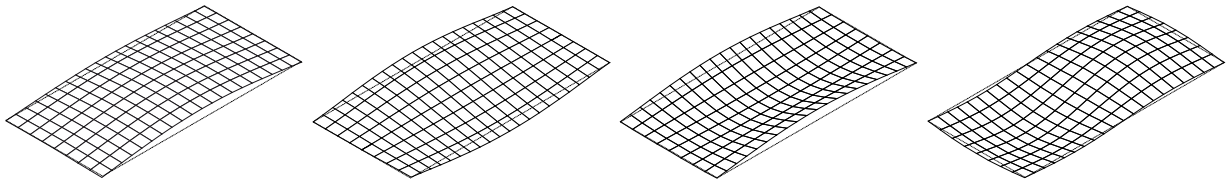

(a) $f_1 = 11.80\,\mathrm{Hz}$ (b) $f_2 = 21.90\,\mathrm{Hz}$ (c) $f_3 = 29.99\,\mathrm{Hz}$ (d) $f_4 = 47.82\,\mathrm{Hz}$

Figure 6: Four mode shapes of the structure

The influence of the soil-structure interaction on the dynamic behaviour was evaluated by means of the deck receptance. The deck receptance was computed by the frequency content of the track response. Fig. 7 shows the vertical displacement at the centre of the mid-span deck due to an impulsive load $P(t) = -1\,\mathrm{N}\,(H(t) - H(t - 0.045\,\mathrm{s}))$ acting on both rails. Fig. 7.(a) shows how the maximum displacement reached during the acting load increased as the soil stiffness decreased. The receptance (Fig. 7.(b)) shows that the response was governed by the first deck bending (symmetric) mode. The first resonant frequencies of the structure ranged from $f_1 = 11.80\,\mathrm{Hz}$, when the soil was not taken into account, to $f_1 = 9.89\,\mathrm{Hz}$ for the soft soil. The damping of the system, obtained from the free vibration response, reached a maximum value $\zeta = 6.4\,\%$ in the soft soil and a minimum value $\zeta = 2\,\%$ when the interaction was not considered. Table 2 summarizes the results for the different soil types considered. The soil-structure interaction led to a decrease in frequencies and an increase in damping ratios.

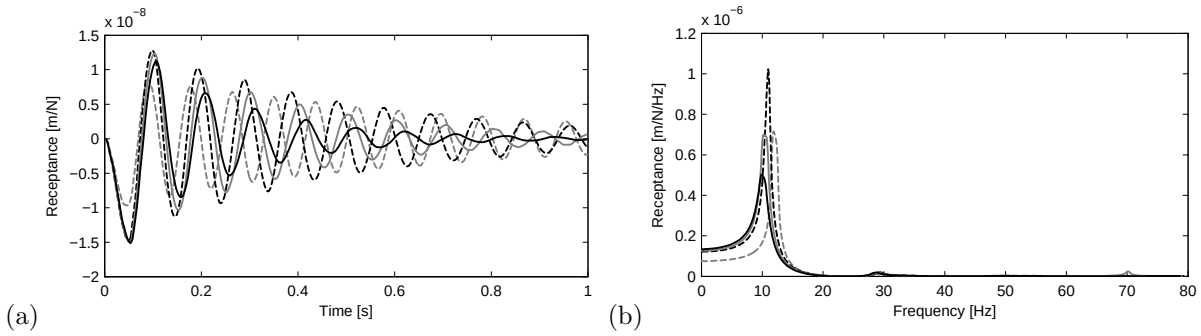

Figure 7: (a) Time history and (b) frequency content of deck receptance for $C_s = \infty$ m/s (grey dashed line), $C_s = 400$ m/s (black dashed line), $C_s = 250$ m/s (grey solid line) and $C_s = 150$ m/s (black solid line)

4.2. Soil-structure vibrations

The resonant condition of a bridge excited by a row of moving forces can be expressed as follows [2, 5]:

$$v_{n,i} = \frac{f_n d}{i} \quad (n = 1, 2, ..., \, i = 1, 2, ...) \tag{17}$$

where $v_{n,i}$ is the resonant train speed, f_n is the n-th resonant frequency of the bridge and d is a characteristic distance between moving loads. Fig. 8 shows the maximum vertical acceleration at the centre of the deck for a range of train speeds between 30 m/s and 130 m/s (108 km/h and 468 km/h, respectively). The deck acceleration was found to increase with train speed. Local maxima were reached at resonant speeds corresponding to the first bending mode shape, considering the distance between bogies $d = 18.7$ m. Fig. 8 shows maximum vibration levels at speed $v_{1,2} = 110.4$ m/s when soil-bridge interaction was not considered. The response of the structure changed substantially when soil-structure interaction was considered. The second resonant speed of the first mode shape decreased to $v_{1,2} = 103$ m/s and $v_{1,2} = 95$ m/s for stiff and medium soil, respectively, due to the change in the dynamic behaviour of the system (Table 2). In addition, the maximum level of acceleration reached in the resonant regime was significantly lower when the soil-structure interaction was considered. No resonant effects occurred with soft soil. In all cases, the maximum acceleration at the centre of the mid-span deck was below $a_{max} = 3.5$ m/s^2 in the range of operating speeds on current high speed lines, that is, the limit set by the European Committee for Standardisation (CEN) [1].

Soil-structure vibrations induced by train passage at the second resonant speed of the first mode of vibration $v_{1,2}$ are analysed below for each soil type. Although the maximum response occurred at the first resonant speed, this speed was much higher than the current operation speed, for example $v_{1,1} = 220.7$ m/s (794 km/h) when soil-structure interaction was not taken into account.

Fig. 9 shows the dynamic amplification factors (DAF) of the soil and the structure due to a HST

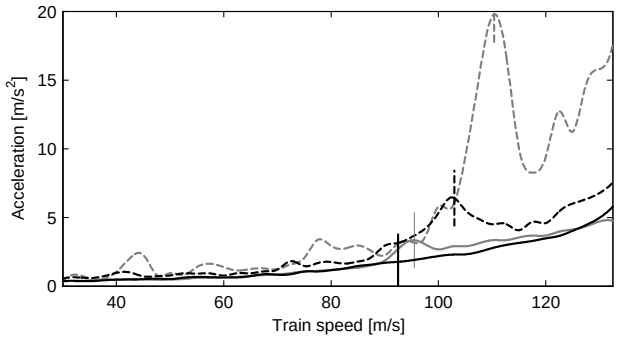

Figure 8: Maximum vertical acceleration at the centre of the mid-span deck for $C_s = \infty$ m/s (grey dashed line), $C_s = 400$ m/s (black dashed line), $C_s = 250$ m/s (grey solid line) and $C_s = 150$ m/s (black solid line). The second resonant speeds of the first mode are marked with vertical lines.

Soil type	c_S [m/s]	f_1 [Hz]	ζ_1	$v_{1,2}$ [m/s]	DAF
Infinitely stiff	-	11.80	0.020	110.4	4.4
Stiff soil	400	11.01	0.034	103	2.3
Medium soil	250	10.16	0.046	95	1.9
Soft soil	150	9.89	0.064	92.5	1.8

Table 2: Summary of soil-bridge interaction according to modal properties and resonant speeds

travelling at the speed $v_{1,2}$ shown in Table 2. The DAF is defined as:

$$DAF = \frac{u_d}{u_s} \tag{18}$$

where u_d are the displacements for the different soil types and train speeds at the time step when the maximum deck response is achieved, and u_s is the maximum static deck displacement without considering soil-bridge interaction. As expected, maximum dynamic amplification was reached when soil-bridge interaction was not considered, and bridge displacements decreased with soil stiffness. As the soil became softer, its influence on bridge response increased. This effect is further described in section 4.3.

Fig. 10 shows the time histories of vertical acceleration at the centre of the mid-span deck for speed $v_{1,2}$ and the acceleration limit for a ballasted track $a = 3.5\,\mathrm{m/s^2}$ [1]. Figs. 10.(a-c) show a gradual increase of the response of the structure with successive bogie passage. The amplification of the response with each bogie passage was greater when soil interaction was not considered and decreased when soil stiffness was lower. There was no evidence of amplification in soft soil (Fig. 10.(d)).

Fig. 11 shows the frequency content of vertical acceleration at the centre of the mid-span deck for train speeds from 30 m/s to 130 m/s. The frequency content was normalized to the acceleration level at the first resonance frequency for a train travelling at $v_{1,2}$ when soil-structure interaction was not considered. Fig. 11.(a) shows a global maximum at the first resonant vibration $f_1 = 11.80\,\mathrm{Hz}$ for the second resonant speed

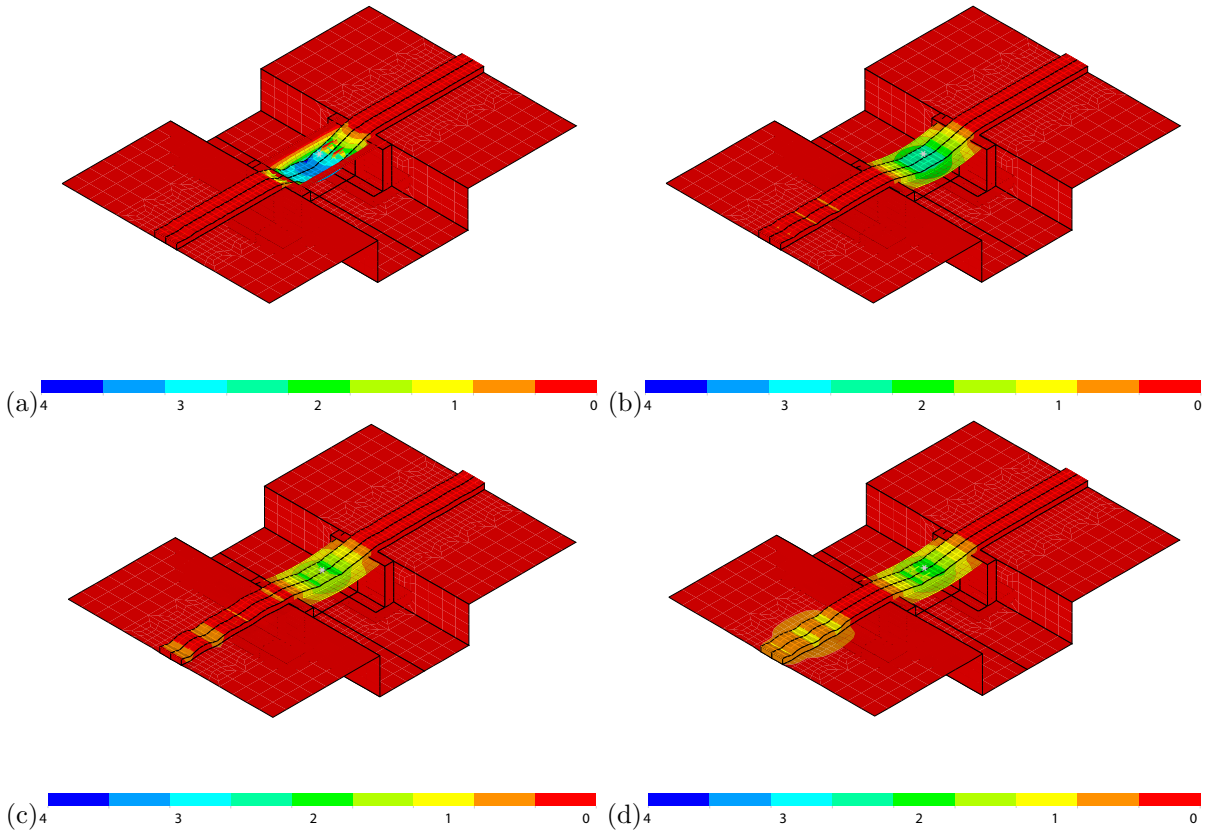

Figure 9: Dynamic amplification factor of ground-structure displacements for a HST travelling at (a) $v = 110.4\,\mathrm{m/s}$, (b) $v = 103\,\mathrm{m/s}$, (c) $v = 95\,\mathrm{m/s}$ and (d) $v = 92.5\,\mathrm{m/s}$ on (a) infinitely stiff soil, (b) hard soil, (c) medium soil and (d) soft soil

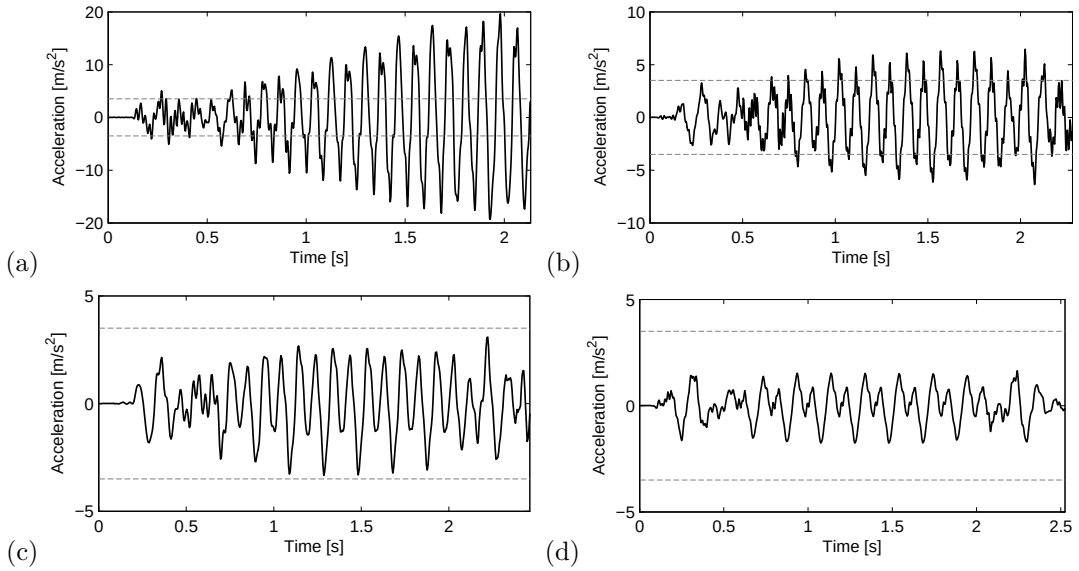

Figure 10: Time histories of vertical acceleration at the centre of the mid-span deck for a HST travelling at (a) $v = 110.4\,\mathrm{m/s}$, (b) $v = 103\,\mathrm{m/s}$, (c) $v = 95\,\mathrm{m/s}$ and (d) $v = 92.5\,\mathrm{m/s}$ on (a) infinitely stiff soil, (b) hard soil, (c) medium soil and (d) soft soil

$v_{1,2} = 110.4\,\mathrm{m/s}$ and local maxima for $v_{1,3}$, $v_{1,4}$, $v_{1,5}$ and $v_{1,6}$. As the soil-bridge interaction increased (Figs. 11.(b-d)), the acceleration level at the bogie passage frequency $f_b = v/l_b$ became dominant and the frequency content of the response of the bridge at the first resonance frequency decreased.

Fig. 12 shows the frequency content of vertical acceleration at a train speed $v_{1,2}$ for the different soil types studied. Maximum vibration level was reached at the first resonance frequency when soil interaction was not considered. The amplification of the resonant response decreased with lower soil stiffness, as well as the relationship between frequency content at the first resonance frequency and bogie passage frequency. Both levels were similar for soft soil. This matched the severity of the response in the resonant regime.

4.3. Abutment support response

Fig. 13 shows the time histories and one-third band spectra of vertical acceleration at the bottom of the first and second support abutments at $v_{1,2}$ for each soil type. The vertical acceleration of the deck is superimposed on the one-third band spectra. Resonant behaviour was reached in the abutment in stiffer and medium soil. Acceleration levels increased with lower soil stiffness and the maximum response was obtained in soft soil, although resonant behaviour was not observed. The first abutment reached higher acceleration vibration levels than the second abutment due to a sudden stiffness change between the track-soil and the track-bridge-soil systems. In addition, the difference between the abutments and deck responses decreased in softer soil, since soil-bridge interaction became dominant.

Fig. 14 shows the time histories and one-third band spectra of the vertical reaction forces at the bottom

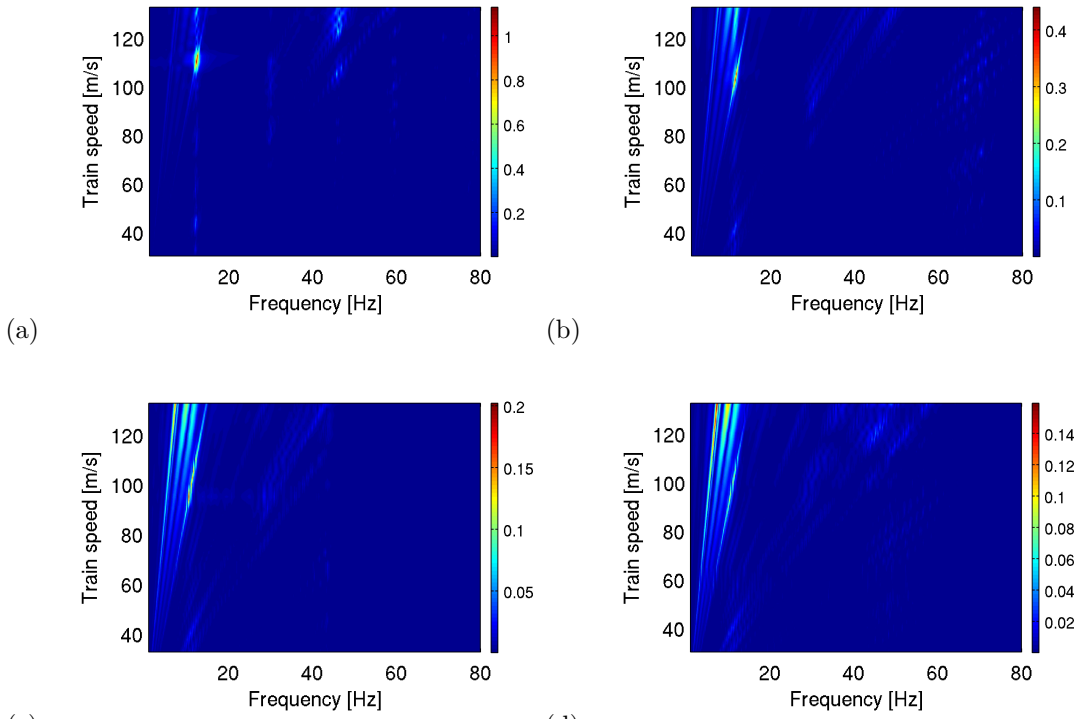

Figure 11: Normalized frequency content of vertical acceleration at the centre of the mid-span deck for a HST travelling from 30 m/s to 130 m/s on (a) infinitely stiff soil, (b) hard soil, (c) medium soil and (d) soft soil

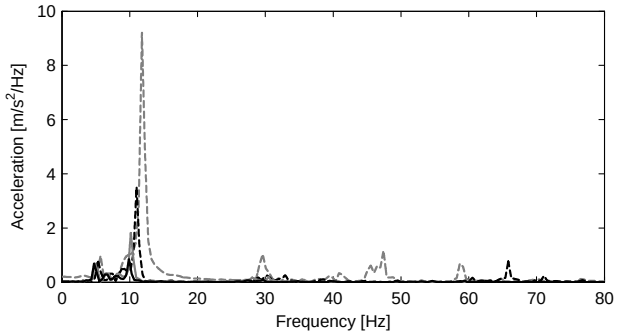

Figure 12: Frequency content of vertical acceleration at the centre of the mid-span deck for a HST travelling at $v = 110.4$ m/s (infinitely stiff soil, grey dashed line), $v = 103$ m/s (hard soil, black dashed line), $v = 95$ m/s (medium soil, grey solid line) and $v = 92.5$ m/s (soft soil, black solid line).

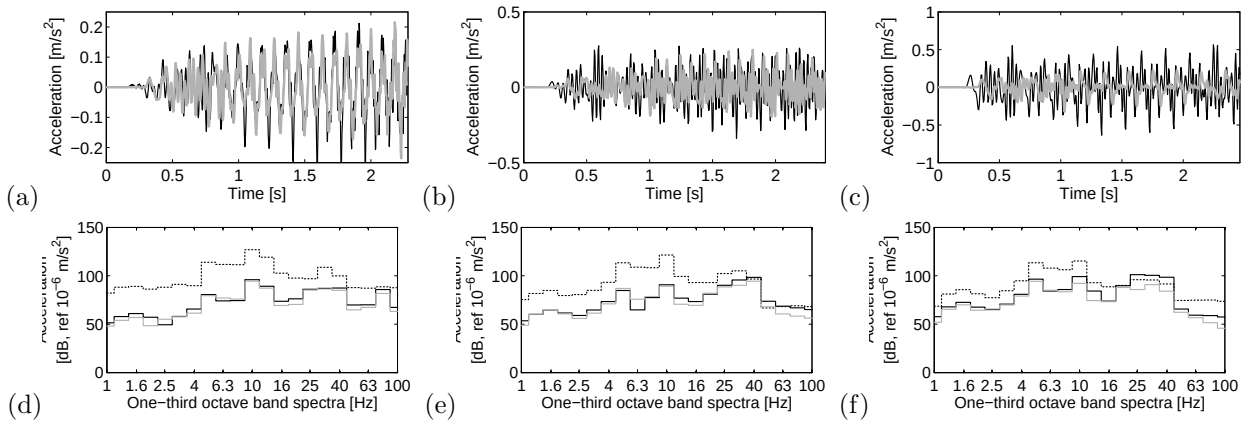

Figure 13: (a-c) Time history and (d-f) one-third band spectra of vertical acceleration at the the bottom of the first abutment support (black solid line) and the second abutment support (grey line) for a HST travelling at (a,d) $v = 103\,\mathrm{m/s}$ ($C_s = 400\,\mathrm{m/s}$), (b,e) $v = 95\,\mathrm{m/s}$ ($C_s = 250\,\mathrm{m/s}$) and (c,f) $v = 92.5\,\mathrm{m/s}$ ($C_s = 150\,\mathrm{m/s}$). The dotted line represents the vertical acceleration of the deck superimposed on the one-third band spectra

of the first and second support abutments for the resonant train speeds. Reaction forces were higher when soil-interaction was not considered. These forces were superimposed on the one-third band spectra. The highest force transmitted to the soil was reached when the resonant regime occurred on stiff soil. In this case, the contribution of high frequencies was noticeable. Reaction forces decreased with soil stiffness and minimum forces were computed on soft soil.

5. Conclusions

This paper presents a numerical model to predict vibrations on railway bridges. The numerical model was based on three-dimensional finite element and boundary element formulations in the time domain. Articulated HSTs were modelled as a multi-body system. It was possible to consider the different excitation mechanisms accurately. The following conclusions can be drawn from the results obtained:

1. Soil-structure interaction leads to changes in dynamic behaviour. The fundamental periods and damping ratios of the response were higher when soil-structure interaction was considered than when it was not.
2. The resonance condition in railway bridges depends on resonance frequencies. Resonant train speeds were lower when soil-bridge interaction was considered. Amplification in the resonant regime was also lower.
3. Therefore, dynamic effects on railway bridges considering soil-structure interaction are an important issue in structure design. Computed bridge deck acceleration is more realistic and the limits set by railway bridge standards could be satisfied with a more slender structure. Moreover, resonance

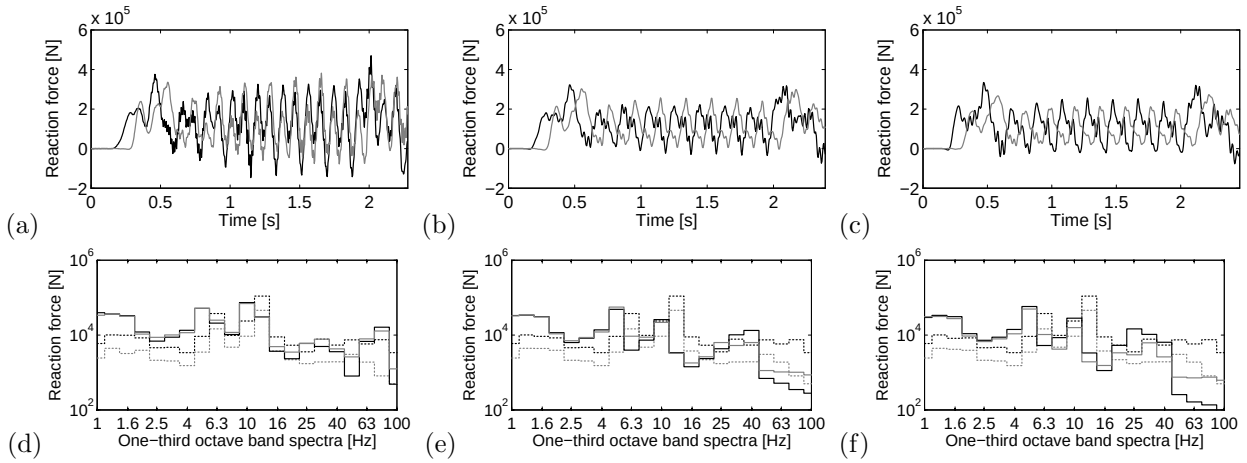

Figure 14: (a-c) Time history and (d-f) one-third band spectra of the vertical reaction forces at the bottom of the entry abutment support (black solid line) and the exit abutment support (grey line) for a HST travelling at (a,d) $v = 103\,\mathrm{m/s}$ ($C_s = 400\,\mathrm{m/s}$), (b,e) $v = 95\,\mathrm{m/s}$ ($C_s = 250\,\mathrm{m/s}$) and (c,f) $v = 92.5\,\mathrm{m/s}$ ($C_s = 150\,\mathrm{m/s}$). The dotted line represents the reaction forces without considering soil interaction superimposed on the one-third band spectra.

effects may occur at lower operation speeds than those predicted when soil-bridge interaction is not considered.

4. The response of the abutment support depends on soil stiffness. This response was higher in soils with lower stiffness. However, the maximum force transmitted to the soil and resonant response were reached in the stiffest soil.

Acknowledgments

This research was financed by the Spanish Ministry of Science and Innovation (*Ministerio de Ciencia e Innovación*) under research project BIA2010-14843. This financial support is gratefully acknowledged. The authors also wish to acknowledge the support provided by the Andalusian Scientific Computing Centre (CICA).

References

[1] European Committee for Standardisation (CEN), Eurocode 1: actions on structures-part 2: traffic loads on bridges. (2008).

[2] L. Frýba, A rough assessment of railway bridges for high-speed trains, Engineering Structures (23) (2001) 548–556.

[3] J. Li, M. Su, The resonant vibration for a simply supported girder bridge under high-speed trains, Journal of Sound and Vibration 224 (5) (1999) 897–915.

[4] S. H. Ju, H. T. Lin, Resonance characteristics of high-speed trains passing simply supported bridges, Journal of Sound and Vibration 267 (5) (2003) 1127–1141.

[5] H. Xia, N. Zhang, W. W. Guo, Analysis of resonance mechanism and conditions of train-bridge system, Journal of Sound and Vibration 297 (3-5) (2006) 810–822.

[6] P. Museros, E. Alarcón, Influence of the second bending mode on the response of high-speed bridges at resonance, Journal of Structural Engineering 131 (3) (2005) 405–415.

[7] P. Museros, M. D. Martínez-Rodrigo, Vibration control of simply supported beams under moving loads using fluid viscous dampers, Journal of Sound and Vibration 300 (1-2) (2007) 292–315.

[8] M. D. Martínez-Rodrigo, J. Lavado, P. Museros, Transverse vibrations in existing railway bridges under resonant conditions: Single-track versus double-track configurations, Engineering Structures 32 (7) (2010) 1861–1875.

[9] M. D. Martínez-Rodrigo, J. Lavado, P. Museros, Dynamic performance of existing high-speed railway bridges under resonant conditions retrofitted with fluid viscous dampers, Engineering Structures 32 (3) (2010) 808–828.

[10] M. D. Martínez-Rodrigo, P. Museros, Optimal design of passive viscous dampers for controlling the resonant response of orthotropic plates under high-speed moving loads, Journal of Sound and Vibration 330 (7) (2011) 1328–1351.

[11] A. V. Pesterev, L. A. Bergman, C. A. Tan, T. C. Tsao, B. Yang, On asymptotics of the solution of the moving oscillator problem, Journal of Sound and Vibration 260 (3) (2003) 519–536.

[12] K. Liu, G. D. Roeck, G. Lombaert, The effect of dynamic train-bridge interaction on the bridge response during a train passage, Journal of Sound and Vibration 325 (1-2) (2009) 240–251.

[13] H. Takemiya, X. C. Bian, Shinkansen high-speed train induced ground vibrations in view of viaduct-ground interaction, Soil Dynamics and Earthquake Engineering 27 (6) (2007) 506–520.

[14] H. Takemiya, Analyses of wave field from high-speed train on viaduct at shallow/deep soft grounds, Journal of Sound and Vibration 310 (3) (2008) 631–649.

[15] M. Ülker-Kaustell, R. Karoumi, C. Pacoste, Simplified analysis of the dynamic soil-structure interaction of a portal frame railway bridge, Engineering Structures 32 (11) (2010) 3692–3698.

[16] O. von Estorff, Dynamic response of elastic blocks by time domain bem and fem, Computers and Structures 38 (3) (1991) 289–300.

[17] O. C. Zienkiewicz, The finite element method, 3rd Edition, McGraw-Hill, 1986.

[18] J. Domínguez, Boundary elements in dynamics, Computational Mechanics Publications and Elsevir Aplied Science, Southampton, 1993.

[19] P. Galvín, J. Domínguez, Analysis of ground motion due to moving surface loads induced by high-speed trains, Engineering Analysis with Boundary Elements 31 (11) (2007) 931–941.

[20] P. Galvín, J. Domínguez, High-speed train-induced ground motion and interaction with structures, Journal of Sound and Vibration 307 (3-5) (2007) 755–777.

[21] N. M. Newmark, A method of computation for structural dynamics, ASCE Journal of the Engineering Mechanics Division 85 (1) (1959) 67–94.

[22] R. W. Clough, J. Penzien, Dynamic of Structures, McGraw-Hill, New York, 1975.

[23] P. Galvín, A. Romero, J. Domínguez, Fully three-dimensional analysis of high-speed traintracksoil-structure dynamic interaction, Journal of Sound and Vibration 329 (24) (2010) 5147–5163.

[24] X. Sheng, C. J. C. Jones, D. J. Thompson, A theoretical model for ground vibration from trains generated by vertical track irregularities, Journal of Sound and Vibration 272 (3-5) (2004) 937–965.

[25] C. Esveld, Modern Railway Track, MRT Productions, Zaltbommel, 2001.

[26] A. Romero, P. Galvín, J. Domínguez, Short span bridges dynamic behaviour account for the vehicle-track-structure-soil dynamic interaction [comportamiento dinámico de viaductos cortos considerando la interacción vehículo-vía-estructura-suelo], Revista Internacional de Metodos Numéricos para Cálculo y Diseño en Ingeniería 28 (1) (2012) 55–63.

[27] S. Y. Chang, Nonlinear error propagation analysis for explicit pseudodynamics algorithm, Journal of Engineering Mechanics ASCE 123 (2003) 841–850.

[28] G. Lombaert, G. Degrande, Ground-borne vibration due to static and dynamic axle loads of intercity and high-speed

trains, Journal of Sound and Vibration 319 (3-5) (2009) 1036–1066, cited By (since 1996) 16.

[29] G. Lombaert, G. Degrande, J. Kogut, S. François, The experimental validation of a numerical model for the prediction of railway induced vibrations, Journal of Sound and Vibration 297 (3-5) (2006) 512–535.

[30] International Organization for Standardization, ISO 8608:1995 Mechanical vibration road surface profiles-reporting of measured data (1995).